Effect of Silicate Pretreatment on Lanthanum Conversion Coating of Hot-dip Galvanized Steel

Shuanghong Zhang[1,], Bo Yang[1], Gang Kong[2], Jintang Lu[2]*

[1] Guangzhou Special Pressure Equipment Inspection and Research Institute, Keyan Road No.9, Huangpu District, Guangzhou 510663, China
[2] School of Material Science and Engineering, South China University of Technology, Wushan Road No.381, Tianhe District, Guangzhou 510640, China
[*]E-mail: zshscut@163.com.

Modified lanthanum conversion coatings were obtained by immersing hot-dip galvanized (HDG) steel sheets that underwent silicate pretreatment in a lanthanum nitrate solution. The results of potentiodynamic polarization and electrochemical impedance spectroscopy (EIS) measurements revealed that silicate pretreatment improved the protective property of the lanthanum conversion coatings, and this conclusion was then corroborated by neutral salt spray (NSS) tests. The morphology and chemical compositions of coatings were examined by scanning electron microscopy (SEM), energy dispersive spectroscopy (EDS), scanning tunnelling microscopy (STM) and Auger electron spectroscopy (AES). The results showed that many silicate particles were dispersed evenly onto the surface of HDG after silicate pretreatment; as a result, the growth of the lanthanum conversion coatings tended to be homogeneous, so that more uniform and compact coatings can be obtained.

1. INTRODUCTION

Hot-dip galvanizing (HDG) is an effective method for preventing atmospheric corrosion of steel products that are widely used in the electric power, transportation and automotive industries and other industrial applications. To improve corrosion resistance and prevent wet storage rust on zinc coatings, chromate salts have been used as effective corrosion inhibitors for HDG steels. However, hexavalent chromium is extremely toxic and harmful to the environment, limiting the use of chromium coatings [1]. Therefore, it is necessary to develop a chromate-free passivation approach. It is well-known that rare-earth salts are effective corrosion inhibitors, and they have been used as passivators to

improve the corrosion protection of many metals such as aluminium and its alloys [2–9], carbon steel [10], zinc and galvanized steels [11–13], and magnesium alloys [14–18]. Rare earth conversion coatings can be obtained by several methods [19] such as electroplating, spray and immersion.

The formation of the rare earth conversion coating has been explained by a cathodic mechanism [20–22]. According to this mechanism, the increase of the local surface pH resulting from the cathodic reactions induces the localized precipitation of rare earth hydroxides, ultimately forming a rough coating. In a previous study[12], the growth behaviour of the lanthanum conversion coating on hot-dip galvanized steel was investigated, and the results indicated that the lanthanum conversion coating on hot dip galvanized steel grew more rapidly at the zinc grain boundaries, and the thicker conversion coating in the vicinity of the grain boundary cracked first, resulting in decreasing protection. Recently, many studies have devoted greater attention to the modification of rare earth conversion coatings by additives [23–24] or by the use of two- or more step treatments to obtain the compound coatings [25–27]. Therefore, by modifying the surfaces of the galvanized coating, such as by preparing alkaline particles on the surface of HDG to induce the precipitation of rare earth hydroxides, more uniform and better corrosion resistance can be obtained by the rare earth coating.

Following the research reported in Ref. [12], in this work, modified lanthanum conversion coatings were obtained by simple immersion of hot-dip galvanized (HDG) sheets in a low concentration silicate solution prior to their immersion in a lanthanum nitrate solution. The effects of the silicate pretreatment on the microstructures and protective properties of the lanthanum conversion coatings were investigated. The growth process of the modified lanthanum conversion coating on the hot-dip galvanized steel was discussed.

2. MATERIALS AND METHODS

2.1 Material and galvanizing

Samples of cold-rolled steel were machined to dimensions of 40 mm × 50 mm × 0.8 mm as the substrates to be galvanized, and the chemical composition of the steel was as follows (% by weight): 0.038 C, 0.03 Si, 0.01 Al, 0.01 Cr, 0.21 Mn, 0.01 S, 0.012 P, 0.01 Ni and balance Fe. The samples were degreased in a hot 10% NaOH solution and then rinsed with water, pickled in a 10% HCl solution and then rinsed with water, fluxed in an aqueous solution composed of 100 g/l $ZnCl_2$ and 150 g/l NH_4Cl at 60 °C for 1 min, dried and dipped into a molten zinc bath (prepared from zinc ingot consisting of 99.995% Zn) at a temperature of 450 °C for 1 min, withdrawn at a constant velocity from the zinc bath and then quenched in cold water immediately. The thickness of the galvanized coating was 40 ~ 50 μm (checked using an STH-1 thickness gauge).

2.2 Silicate pretreatment and lanthanum conversion coatings

The silicate solution (0.5 g/L of SiO_2 with the SiO_2/Na_2O molar ratio of 3.5) used in this study was prepared by dissolving a specific amount of silica powder (diameter 20 nm, amorphous) in a

strong NaOH solution. The mixed solution was then diluted to the required concentration and a pH of 9.98. The solutions were stored for 2 days in sealed polypropylene vials prior to use. The lanthanum solution was composed of 20 g/l La(NO$_3$)$_3$·6H$_2$O and 10 ml/l 30% (v/v) H$_2$O$_2$.

Prior to deposition, the HDG samples were thoroughly rinsed with ethanol and deionized water and then pretreated in the silicate solution for 1 min at ambient temperature, followed by immersion in the lanthanum solution at 70 °C for durations ranging from 10 to 1800 s and then drying in air. The method for the preparation of the lanthanum conversion coatings used in this work is similar to those reported in the literature [12]. SLX and LX were used to denote the lanthanum conversion coatings with and without the silicate pretreatment, respectively, where the number "X" is the corresponding time in seconds, and HDG denotes the untreated hot dip galvanized sample.

2.3 Characterization

The surface morphology and microstructure of the samples were observed by scanning electron microscopy (SEM), using a Philips XL-30 instrument (FEI Company, Hillsboro, Oregon, USA) equipped with an energy dispersive spectrometer (EDS) and by scanning tunnelling microscopy (STM, Nanoscope IIIA, Santa Barbara, USA) with Pt/It tips (90/10, 0.25 mm diameter). Auger electron spectroscopy (AES, PHI-550 ESCA/SAM, PerkinElmer, USA) was used to analyse the depth profile to describe the elemental depth distribution and coating thickness. The data were obtained by an Ar ion beam accelerated at 2 kV, with a sputtering rate of 10 nm/min that was calibrated by a 100 nm-thick Ta$_2$O$_5$ film, and the sputtered area was 1 mm $\times$ 1 mm.

2.4 Property evaluation of the coating

The protection property of the samples was evaluated using a CHI640B electrochemical measurement work station in a conventional three-electrode electrochemical cell, where a platinum foil and a saturated calomel electrode (SCE) were used as the counter and the reference electrodes, respectively, in addition to a working electrode (exposed area of 1 cm^2). Prior to the measurements, the working electrode was immersed in 5 wt.% NaCl for approximately 30 min to obtain a stable open circuit potential. Electrochemical impedance spectra (EIS) measurements were performed in the frequency range from 100 kHz to 0.01 Hz using a sinusoidal alternating potential signal with an amplitude of 10 mV under open circuit conditions. The potentiodynamic polarization measurements were performed at a scanning rate of 1 mV/s. The measurement data were analysed using the CHI640B software package and fitted using the ZVIEW (version 2.1C) software.

Neutral salt spray (NSS) tests were conducted in a salt spray test chamber (YWX/Q150). using a 5 wt.% NaCl solution with pH 6.50–7.00 at (35 ± 2) °C. The samples were placed perpendicularly at 30° angles. Each spray cycle consisted of 8 h of spray and a 16 h dry period. The deterioration of the samples was estimated by a grid method in which the corroded area was examined after a certain spray time. All data from the NSS tests are the average of three measurements.

3. RESULTS AND DISCUSSION

3.1 Electrochemical characteristics

The potentiodynamic polarization curves of the untreated HDG sample and the silicate pretreated samples immersed in the lanthanum salt solution for different durations in 5 wt.% NaCl solution are presented in Fig. 1. After immersion in the lanthanum salt solution, both the anodic and cathodic branches of the polarization curves moved towards the direction of decreasing current, suggesting that the anodic and cathodic processes of zinc corrosion were inhibited, and the inhibition effects for the cathodic process were greater than those for the anodic process, in agreement with the results for the single lanthanum conversion coating [12].
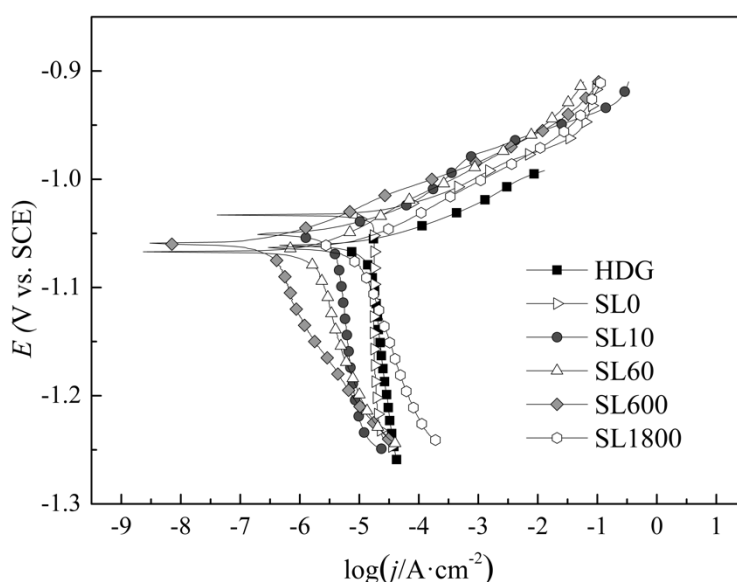

Figure 1. Potentiodynamic polarization curves of the HDG sample and silicate pretreated samples immersed in a lanthanum salt solution for different durations in a 5 wt.% NaCl solution.

Table 1. Electrochemical parameters obtained from the potentiodynamic polarization curves shown in Figure 1.

Sample	E_{corr}(V/SCE)	β_a (mV/dec)	β_c (mV/dec)	R_p/k$\Omega\cdot$cm^2	j_{corr}/μA$\cdot$cm^{-2}
HDG[*]	-1.06	17	-184	0.58	13.00
SL0	-1.02	21	-215	0.27	33.02
SL10	-1.05	18	-203	2.19	3.65
SL60	-1.06	20	-172	4.88	1.74
SL600	-1.06	16	-155	23.78	0.29
SL1800	-1.06	20	-181	3.90	2.26

The electrochemical parameters derived from the polarization curves. The results of the open circuit potential E_{corr}, the corrosion current density j_{corr}, the polarization resistance R_p, the anodic and cathodic Tafel slopes, β_a and β_c, calculated by the Tafel extrapolation method, are listed in Table 1.

As shown in Figure 1 and Table 1, the anodic slopes β_a were little changed whereas the slopes of the cathodic branches were more polarised suggesting that the corrosion rate was under cathodic control (oxygen diffusion). The corrosion current density j_{corr} decreased with increasing lanthanum treatment time up to 600 s and then increased with longer time, so that the SL600 sample showed the lowest j_{corr} and the highest protection property. In addition, after the silicate pretreatment, the polarization resistance R_p decreased and j_{corr} increased for SL0 compared to HDG, implying that a complete silicate coating with protection property was not formed on the zinc coating after pretreatment with a low concentration of silicate.

Nyquist plots of these samples in a 5 wt.% NaCl solution are presented in Fig. 2(a). The impedance diagrams for all samples consisted of two overlapping semicircles that were depressed towards the real axis. For HDG and SL0, the very low frequency inductive loop is due to the zinc dissolution process [12]. The appropriate equivalent circuit consistent with the Nyquist plots is presented in Fig. 2(b). In this equivalent circuit, R_s is the electrolyte resistance, R_f and CPE_f are the resistance and capacitance associated with the coatings, respectively, and R_{ct} and CPE_{dl} are the charge transfer resistance and the double layer capacitance, respectively, where the constant phase elements (CPE) were introduced to replace the capacitors to improve the fitting. For HDG, R_f can be related to the formation of corrosion products composed of zinc oxides/hydroxychlorides [28, 29].
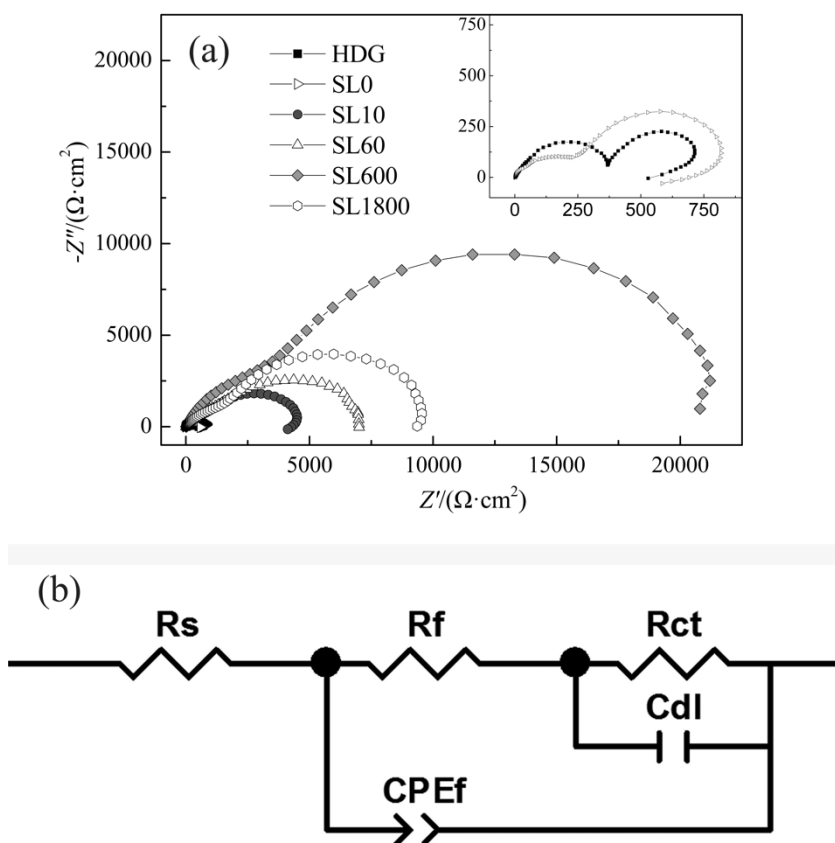

Figure 2. Nyquist plots (a) and equivalent circuit (b) of the HDG sample and La coatings with and without silicate pretreatment in a 5 wt.% NaCl solution.

To interpret the equivalent circuit, the fitted experimental data are listed in Table 2. As shown in Table 2, as the immersion time increased to 600 s, R_f and R_{ct} increased, while CPE_f and CPE_{dl} decreased, indicating that the coating became more thick and compact. The increase of the exponent (n) indicated that the electrode surface became increasingly homogeneous.[30] In addition, R_f of the SL0 sample was smaller than that of the HDG sample. The variation tendency of the R_f, R_{ct} was in agreement with the variation of the electrochemical parameters R_p derived from the potentiodynamic polarization, and maximum values were obtained for the immersion time of 600 s.

Table 2. Fitted parameters obtained from the EIS curves and the equivalent circuit in Figure 2.

Sample	R_f/kΩ·cm^2	$Y_0(CPE_f)$ /×10^{-6}(Ω^{-1}·cm^{-2}·s^{-n})	$n(CPE_f)$	R_{ct}/kΩ·cm^2	C_{dl} /mF·cm^{-2}
HDG	0.41	30.81	0.80	0.37	1.54
SL0	0.22	11.28	0.79	0.57	0.28
SL10	1.31	45.40	0.84	3.08	0.24
SL60	3.24	44.19	0.85	3.12	0.15
SL600	13.71	20.81	0.92	17.90	0.05
SL1800	3.57	56.89	0.71	7.16	0.09

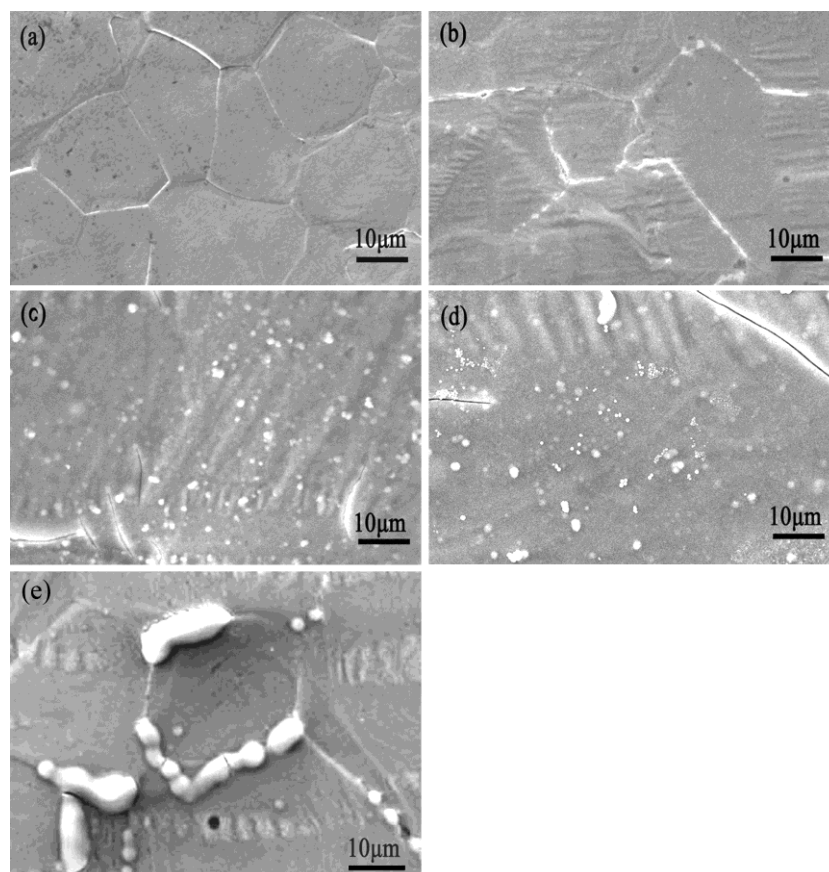*3.2 Surface morphology of the samples*

Figure 3. SEM images of samples (a) SL0, (b) SL60, (c) SL600, (d) SL1800 and (e) La60.

SEM observation showed that zinc grains were clearly visible on the surface of the silicate-pretreated sample SL0 (Fig. 3(a)). The zinc grain boundaries became unclear after immersing the silicate pretreated sample in the lanthanum salt solution for 60 s, and the surface of the coating became flatter (Fig. 3(b)). After increasing the immersion time to 600 s, the zinc grain boundaries disappeared, and few small cracks appeared on the flat surface (Fig. 3(c)); the cracks increased with further increase of the immersion time (Fig. 3(d)). It is important to note that the early growth of the modified La conversion coating in the present work was different from that of the single La conversion coating without the silicate pretreatment; the former grew uniformly, while the latter grew more rapidly in the vicinity of the zinc grain boundaries (Fig. 3(e)) where the cracks occurred first [12].

In further observation by STM, a mass of small raised dots (particles) was observed on the surface of the silicate pretreated sample SL0, as shown in Fig. 4(a). Upon increasing the immersion time in the La solution, the size of these particles increased, leading to the formation of cellular structures that were uniformly distributed on the surfaces of the samples (Figs. 4(b), (c) and (d)). It can be speculated that the La compounds may be deposited preferentially on these raised dots.
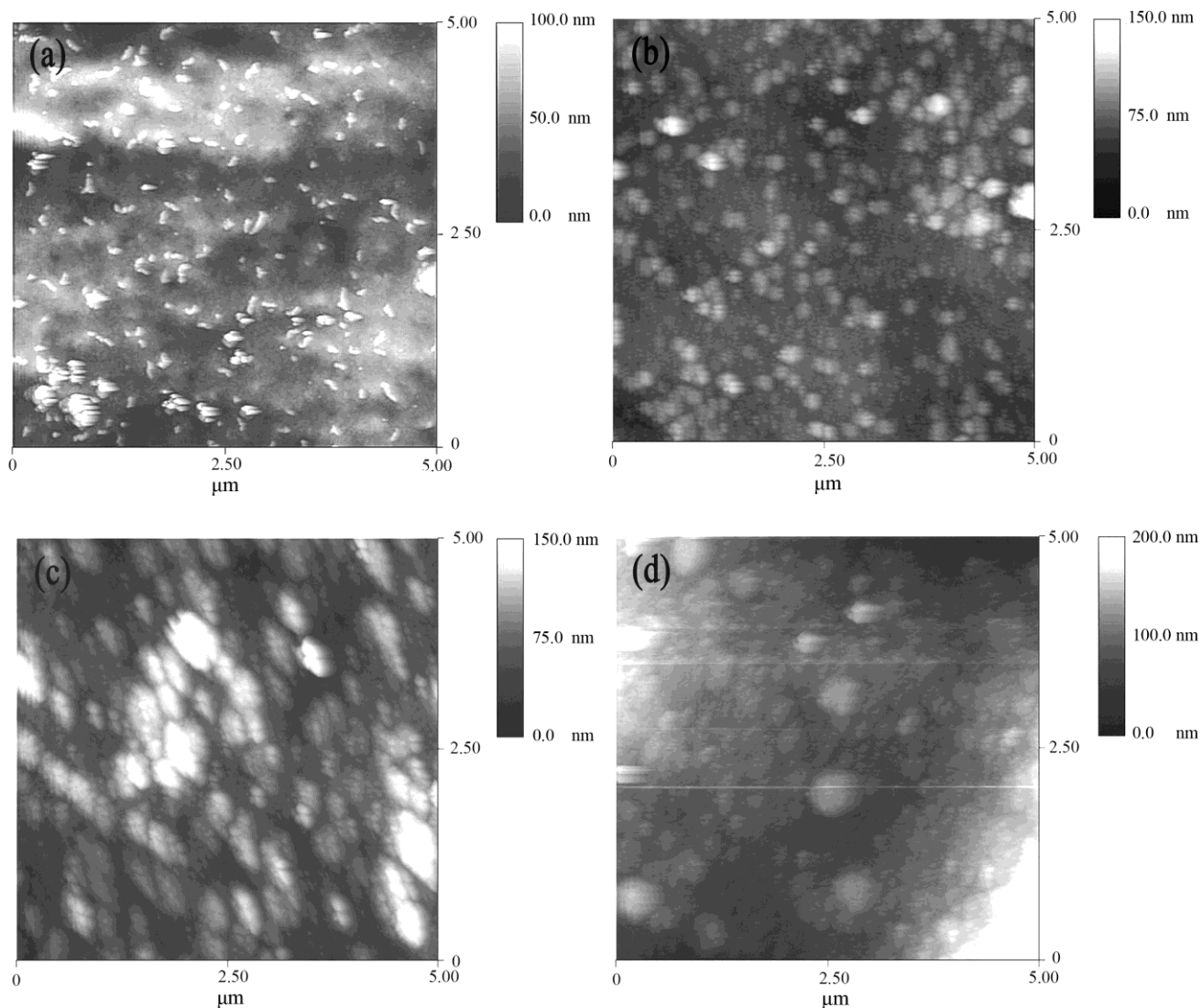

Figure 4. STM images of samples (a) SL0, (b) SL10, (c) SL60 and (d) SL600.

3.3 Chemical composition of the coatings

Fig. 5 shows the AES composition depth profile curve of the SL60 sample, and it is observed that the surface mainly contained La, O and a smaller amount of Zn, while the Si signal was weaker than the detection limit and is not shown in the figure. In initial sputtering, high La and O contents were evident at the top of the surface (approximately 40 at.% and 50 at.%, respectively). With increasing sputtering time, the La content remained approximately 40 at.% up to 500 s, and then decreased gradually and disappeared after approximately 2000 s. Based on the rate and time of argon ion sputtering, the thickness of the SL60 coating is approximately 330 nm.
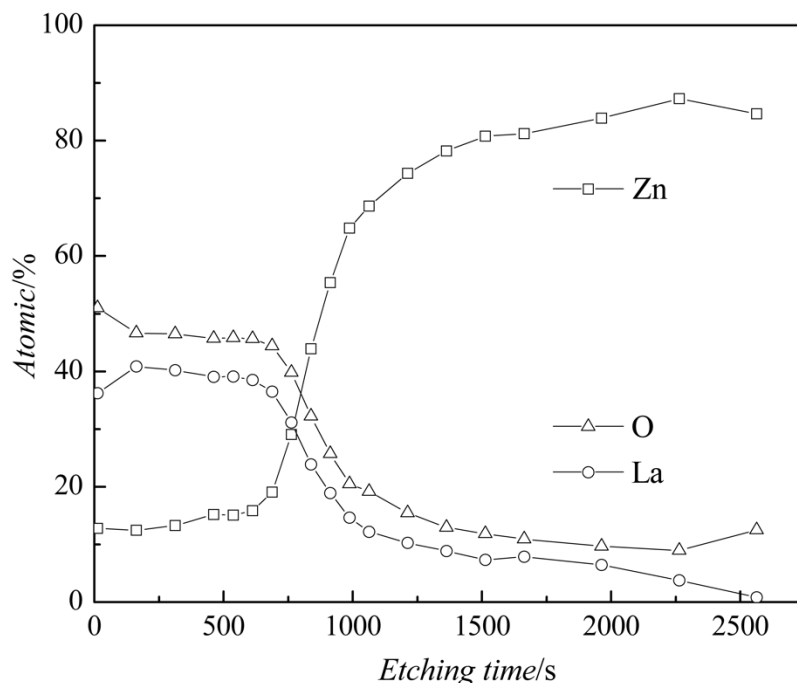

Figure 5. AES composition depth profile curves of the SL60 conversion coating.

The EDS results are shown in Table 3. For EDS, the signals originate from a region of approximately 1 μm³ beneath the sample surface, and the thickness of the conversion coatings and the size of the raised dots are much smaller than 1 μm. Therefore, the contents of La and Si determined by EDS were smaller than the actual contents of the coatings and the raised dots, respectively. However, the higher La content corresponds to the thicker conversation coating, and the increase of the La content corresponds to the increased coating thickness. The data presented in Table 3 show that the La content gradually increased with increasing immersion time, corresponding to the growth of the coatings.

In addition, as shown in Table 3, for the samples immersed in the lanthanum solution for 0–60 s, the Si element was detected, indicating that the silicate was deposited on the pretreated surface. The Si content of EDS decreased with increasing immersing time, possibly because the escape depth of the Si signal increased with the increase in the thickness of the La conversion coating, decreasing the escaped Si signal. For samples SL600 and SL1800, no Si content was observed, corresponding to the

Si signal being weaker than the detection limit rather than to the absence of Si.

Table 3. EDS chemical compositions (at.%) of various samples.

Sample	Element				Note
	Zn	**O**	**La**	**Si**	
SL0	77.90	20.83	0.00	1.27	Silicate particles on Zn coating
SL1	69.94	29.05	0.33	0.68	La coating formed on silicate particles
SL3	74.84	23.98	0.64	0.54	La coating formed on silicate particles
SL10	76.83	22.10	0.85	0. 22	La coating growth
SL60	74.53	24.23	1.06	0.18	La coating growth
SL600	22.61	66.43	10.96	0.00	La coating growth
SL1800	8.13	72.72	19.15	0.00	La coating growth and cracking

3.4 Discussion

According to the methods published in a previous study [12], La conversion coatings are prepared by immersing HDG steel in a lanthanum solution with 20 g/l $La(NO_3)_3 \cdot 6H_2O$ and 10 ml/l 30% (v/v) H_2O_2 at 70 ℃ for durations ranging from 10 s to 240 min, with the results observed using AES, SEM and EIS techniques. It was shown that the La conversion coating grows more rapidly in the vicinity of the zinc grain boundary; the local conversion coating in the vicinity of the grain boundary is cracked first, resulting in the decreased protective property. Regardless of the use of the silicate pretreatment, with increasing immersion time, the protective property of the La conversion coatings gradually increased in the early growth stage and then decreased when cracks developed. Furthermore, there were no significant changes in the La content on the coating surface as measured by EDS and in the coating thickness as measured by AES.

However, a significant difference between the coatings obtained with and without the use of the silicate pretreatment was observed in the initial stage of the La precipitation. For the single La coating without the pretreatment, the La precipitated preferentially near the Zn grain boundary, resulting in an uneven coating surface and early cracks (on sample L10) [12]. Whereas after pretreatment, the La precipitated preferentially on the diffuse silicate particles, resulting in a more uniform and compact coating with enhanced protective property, and no cracks were observed on the sample immersed in the lanthanum solution for 60 s.

To evaluate the effect of the silicate pretreatment on the protective property of the lanthanum conversion coatings, the evolution of the total resistance R_{total} ($R_f + R_{ct}$) for lanthanum coatings with and without the silicate pretreatment as a function of the immersion time is shown in Fig. 6, and it is observed that the values of R_{total} for the lanthanum coating with the silicate pretreatment were always much higher than those for the coating without the pretreatment for any given treatment time.

Neutral salt spray (NSS) tests were used to compare the protective properties of the lanthanum coating samples immersed for 600 s with and without the silicate pretreatment, and the untreated HDG

sample and the chromate coated sample (Cr) were used for comparison. The chromate conversion coating was obtained by immersing the HDG sample in 2 g/l $Na_2Cr_2O_7$ solution at 30 °C for 1 min (this process has been widely adopted for batch hot dip galvanizing).
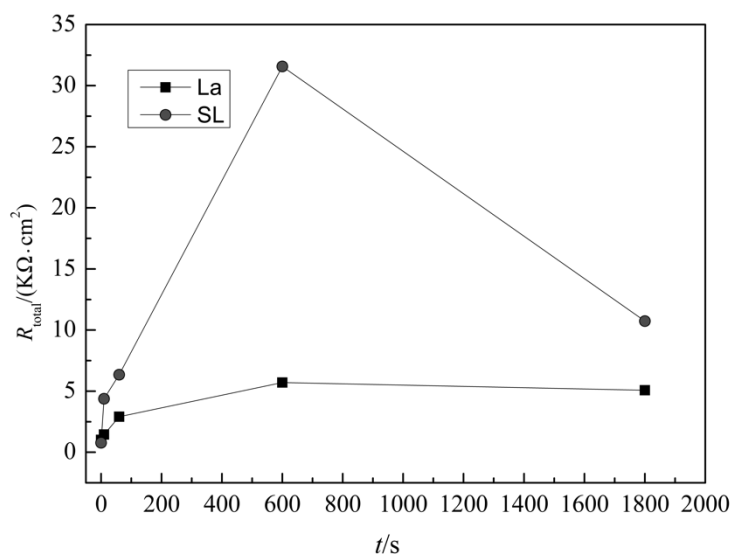

Figure 6. R_{total} variation as a function of immersion time for the La coatings with and without the silicate pretreatment.
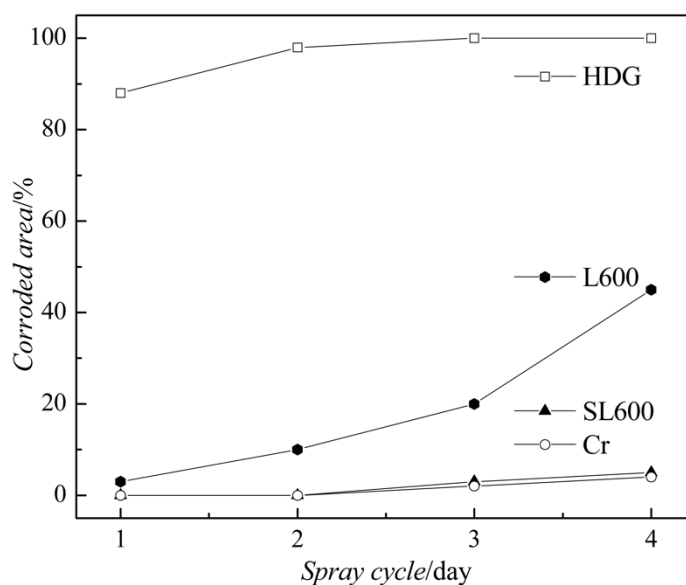

Figure 7. NSS test results for the HDG, L600, SL600 and chromate coating samples.

The results are shown in Fig. 7. After one cycle of spraying, the HDG sample was severely corroded, and almost 90% of its surface was covered by white rust, while the corrosion area on the L600 coating was approximately 3%, and there was no detectable sign of corrosion on the SL600

coating and the chromate coating. After four cycles of spraying, the corrosion area on the L600 coating was approximately 45%, whereas the corrosion area of only 5% was observed on the SL600 coating, showing anti-corrosion performance that is the same as that of the chromate coating.

According to the above EDS results, some silicate was deposited on the surface of the pretreated SL0 sample; however, the R_{total} value of SL0 was very small (less than 1 k$\Omega \cdot$cm^2) (Table 2). Generally, to obtain the silicate conversion coating with an enhanced corrosion resistance, the concentration of the silica in the adopted silicate solution was 100 times greater than that used in the present work, and in that case, the R_{total} value was dozens of k$\Omega \cdot$cm^2 [31–33]. It appears that the low concentration of the alkalic silicate solution used in this work resulted in the discontinuous silicate precipitation rather than the continuous silicate conversion coating. The silicate deposits on the Zn coating mainly consist of zinc silicate and SiO_2 [31], and reactive Si-OH groups are present on the surface of the nanosized silicate particles, favouring the La precipitation. The La compounds precipitated preferentially at these dispersed silicate particles, resulting in a uniform and compact lanthanum coating, where the effect of the silicate pretreatment on the lanthanum coating is similar to the effect of the surface conditioning before the metal phosphating for refining or decreasing crystal size of the phosphate coating [34, 35].

4. CONCLUSIONS

The influence of the silicate pretreatment on the microstructure and protective property of the lanthanum conversion coatings on the hot dip galvanized steel was investigated. Pretreatment with a silicate solution of low concentration was found to be an effective approach for increasing the uniformity and compactness of the lanthanum conversion coating on the hot dip galvanized steel. The results obtained by electrochemical measurements and NSS tests showed that pretreatment with the silicate solution significantly improves the protective performance of lanthanum conversion coatings.

References

1. C. Desai, K. Jain and D. Madamwar, *Bioresour. Technol.*, 99 (2008) 6059.
2. J. Qi, T. Hashimoto, J. Walton, X. Zhou, P. Skeldon and G. E. Thompson, *J. Electrochem. Soc.*, 163 (2016) C25.
3. S. Ershov, M. E. Druart, M. Poelman, D. Cossement, R. Snyders and M. G. Olivier, *Corros. Sci.*, 75 (2013) 158.
4. L. Paussa, F. Andreatta, N. C. R. Navarro, A. Durán, L. Fedrizzi and *Electrochim. Acta*, 70 (2012) 25.
5. J. L. Tang, Z. Z. Han, Y. Zuo and Y. M. Tang, *Appl. Surf. Sci.,* 257 (2011) 2806.

6.   B. Valdez, S. Kiyota, M. Stoytcheva, R. Zlatev and J. M. Bastidas, *Corros. Sci.*, 87 (2014) 141.
7.   M. Machkova, E.A. Matter, S. Kozhukharov and V. Kozhukharov, *Corros. Sci.*, 69 (2013) 396.
8.   F. Andreatta, M. E. Druart, A. Lanzutti, M. Lekka, D. Cossement, M. G. Olivier and L. Fedrizzi, *Corros. Sci.*, 65 (2012) 376.
9.   M. Ozawa, K. I. Araki, *Surf. Coat. Tech.*, 271 (2015) 80.
10. Y. H. Zhu, J. Zhuang, Y. S. Yu and X. G. Zeng, *J. Rare Earths*, 31 (2013) 734.
11. S. Roselli, N. Bellotti, C. Deyá, M. Revuelta, B. D. Amo and R. Romagnoli, *J. Rare Earths*, 32 (2014) 352.
12. S. H. Zhang, G. Kong, J. T. Lu, C. S. Che and L.Y. Liu, *Surf. Coat. Tech.*, 259 (2014) 654.
13. D. G. Wu, S. H. Yan, Z. G. Wang, Z. Q. Zhang, R. Y. Miao and X. W. Zhang, D. H. Chen, *J. Rare Earths*, 32 (2014) 663.
14. S. S. Jamali, S. E. Moulton, D. E. Tallman, Y. Zhao, J. Weber and G. G. Wallace, *Electrochem. Commun.*, 76 (2017) 6.
15. S. Pommiers, J. Frayret, A. Castetbon and M. Potin-Gautier, *Corros. Sci.*, 84 (2014) 135.
16. C. E. Castano, M. J. O'Keefe and W. G. Fahrenholtz, *Surf. Coat. Tech.*, 246 (2014) 77.
17. X. Jiang, R. G. Guo and S. Q. Jiang, *Appl. Surf. Sci.*, 341 (2015) 166.
18. L. Chen, C. G. Chen, N. N. Wang, J. M. Wang and L. Deng, *Rare Metal Mat. Eng.*, 44 (2015) 333.
19. C. E. Castano, M. J. O'Keefe and W. G. Fahrenholtz, *Curr. Opin. Solid St. M.*, 19 (2015) 69.
20. M. A. Arenas, J. J. D. Damborenea, *Surf. Coat. Tech.*, 187 (2004) 320.
21. K. Aramakik, *Corros. Sci.*, 43 (2001) 2201.
22. M. F. Montemor, A. M. Simões and M. G. S. Ferreira, *Prog. Org. Coat.*, 44 (2002) 111.
23. G. Kong, L. Y. Liu, J. T. Lu, C. S. Che and Z. Zhong, *Corros. Sci.,* 53 (2011) 1621.
24. L. Lei, J. Shi, X. Wang, D. Liu and H. Xu, *Appl. Surf. Sci.*, 376 (2016) 161.
25. Y. J. Qiao, W. P. Li, G. X. Wang and X. H. Zhang, *J. Rare Earths*, 33 (2015) 647.
26. B. Ramezanzadeh, H. Vakili and R. Amini, *J. Ind. Eng. Chem.*, 30 (2015) 225.
27. H. Vakili, B. Ramezanzadeh and R. Amini, *Corros. Sci.*, 94 (2015) 466.
28. C. Cachet, F. Ganne, S. Joiret, G. Maurin, J. Petitjean, V. Vivier and R. Wiart, *Electrochim. Acta*, 47 (2001) 509.
29. C. Cachet, F. Ganne, S. Joiret, G. Maurin, J. Petitjean, V. Vivier and R. Wiart, *Electrochim. Acta*, 47 (2002) 3409.
30. A. V. Benedeti, P. T. A. Sumodjo, K. Nobe, P. L. Cabot and W. G. Proud, *Electrochim. Acta*, 40 (1995) 2657.
31. M. R. Yuan, J. T. Lu and G. Kong, *Surf. Coat. Tech.*, 204 (2010) 1229.
32. M. R. Yuan, J. T. Lu and G. Kong, C S. Che, *Surf. Coat. Tech.*, 205 (2011) 4466.
33. F. Jamali, I. Danaee, and D. Zaarei, *Mater. Corros.*, 66 (2015) 459.
34. M. Wolpers, J. Angeli, *Appl. Surf. Sci.*, 179 (2001) 281.
35. I. V. Roy, H. Terryn and G. Goeminne, *Colloids Surf., A: Physicochemical and Engineering Aspects*, 136 (1998) 89.